TYPE 6 SECRETION

In situ architecture, function, and evolution of a contractile injection system

Désirée Böck,[1]* João M. Medeiros,[1]* Han-Fei Tsao,[2] Thomas Penz,[2]† Gregor L. Weiss,[1] Karin Aistleitner,[2]‡ Matthias Horn,[2]§ Martin Pilhofer[1]§

Contractile injection systems mediate bacterial cell-cell interactions by a bacteriophage tail–like structure. In contrast to extracellular systems, the type 6 secretion system (T6SS) is defined by intracellular localization and attachment to the cytoplasmic membrane. Here we used cryo-focused ion beam milling, electron cryotomography, and functional assays to study a T6SS in *Amoebophilus asiaticus*. The in situ architecture revealed three modules, including a contractile sheath-tube, a baseplate, and an anchor. All modules showed conformational changes upon firing. Lateral baseplate interactions coordinated T6SSs in hexagonal arrays. The system mediated interactions with host membranes and may participate in phagosome escape. Evolutionary sequence analyses predicted that T6SSs are more widespread than previously thought. Our insights form the basis for understanding T6SS key concepts and exploring T6SS diversity.

Contractile injection systems (CISs) deliver effectors to mediate bacterial cell-cell interactions. Their structural components are homologous to the contractile tails of phages (*1*). CISs consist of an inner tube surrounded by a contractile sheath, a spike capping the inner tube, and a baseplate complex at the base of the sheath. Sheath contraction propels the inner tube into the target. Two modes of action divide CISs into "extracellular CISs" (eCISs) and "type 6 secretion" (T6S) systems (T6SSs). eCISs resemble headless phages; they are released into the medium and bind to the target cell surface. Examples are antibacterial R-type bacteriocins (*2*), insecticidal antifeeding prophages (Afps) (*3*), and metamorphosis-inducing structures (MACs) (*4*). By contrast, the T6SS is defined by its cytoplasmic localization and anchoring to the inner membrane (*5*–*9*).

Amoebophilus asiaticus (hereafter referred to as *Amoebophilus* or amoebophili) is an obligate intracellular bacterial symbiont of amoebae (*10*). The *Amoebophilus* genome does not encode known secretion systems (*11*); however, it contains a gene cluster with similarities to that of Afps (*12*). We reasoned that the Afp-like gene cluster might encode a system that would give insight into T6SS structure, function, and evolution.

To investigate whether *Amoebophilus* produced any CISs, we imaged bacterial cells that were purified from infected amoeba cultures by electron cryotomography (ECT). Fifty percent of the imaged cells (n = 92) contained phage tail–like assemblies. Like T6SSs and unlike eCISs, the structures were always located in the *Amoebophilus* cytoplasm and attached to the cytoplasmic membrane. The structures were always found in bundles of 2 to 34 parallel individual systems (8 on average; Fig. 1, A to C; fig. S1, A to D; and movie S1). Cells contained either one or two (85%) bundles (Fig. 1D and fig. S1E). Inside a bundle, the structures were arranged in ordered hexagonal arrays (Fig. 1, E and F). Extended and contracted conformational states could be distinguished by differences in length (242 ± 7 nm, n = 254, and 122 ± 6 nm, n = 153, respectively), diameter (14 ± 2 nm and 19 ± 2 nm, respectively), and surface properties of the sheath (helical ridges on the contracted structures) (Fig. 1, B and C, and fig. S1, F to I). The narrow distribution of sheath lengths indicates a mechanism for length control. In addition, not all structures inside an array appeared to fire together (Fig. 1, B to D and F, and fig. S1E).

The arrays of contractile structures were encoded by the *Amoebophilus* Afp-like gene cluster. Twelve of its components were detected in a sheath preparation (table S1). Sheath structures were labeled by specific antibodies (fig. S1, J and K). Furthermore, tomograms of purified sheath revealed contracted sheaths whose structure (fig. S1, L and M) and dimensions (length 115 ± 7 nm, diameter 19 ± 2 nm, n = 51) were consistent with the structures observed in situ (fig. S1, F to I).

To observe macromolecular details, we averaged subvolumes of extended T6S-like machines (Fig. 2, A to K, and movies S2 and S3). The structure revealed three major modules: a sheath-tube assembly, a baseplate, and an anchoring complex (Fig. 2, A to I). This segmentation was supported by the comparison of the average with the structure of the minimal composition of a contractile injection system derived from the T4 phage tail (*13*) (Fig. 2B). All three modules showed sixfold rotationally symmetric features (fig. S2). Densities for the inner tube (7 nm diameter) and sheath (14 nm diameter) could be clearly discerned (Fig. 2, A and I). The baseplate was overall hexagonal (Fig. 2, G and H) and established connections with baseplates of neighboring structures, thereby coordinating multiple systems in hexagonal arrays (Fig. 2, J and K). The central baseplate region featured additional densities that reinforced in a threefold symmetrized average (fig. S2, I to M). The anchoring complex consisted of a six-footed platform that attached the baseplate to the inner membrane (Fig. 2, A and D to F). Densities whose dimensions were consistent with a spike complex (*14*) were seen capping the inner tube and protruded through the centers of baseplate and anchor (Fig. 2, A and B and E to G). The averages lacked densities that would indicate the presence of an elaborate trans-envelope complex (Fig. 2A and fig. S2, A and E to G) such as TssJLM (*9*).

The T4 phage baseplate triggers sheath contraction by a large-scale conformational change (*13*). We therefore calculated an average of contracted structures (Fig. 2, L to R, and movies S4 and S5). Again, sheath, baseplate, and anchor modules were identified (Fig. 2, L to R). All three modules revealed pronounced conformational changes as compared to the extended state (movie S6). Similar to the *Vibrio cholerae* T6SS (*5*), the sheath diameter increased upon contraction, along with the appearance of helical surface ridges and the disappearance of the inner tube (Fig. 2, I and R). The baseplate showed a widening and a loss of densities in the center (Fig. 2, G and H and P and Q). Likewise, the anchoring platform showed lateral expansion (distance between opposing feet at the inner membrane increased from 16 to 19 nm) and a loss of the spike density in the center (Fig. 2, E and F and N and O). On a larger scale, the spacing between contractile structures increased from 22 nm between extended structures to 30 nm between contracted structures.

We then tested whether the *Amoebophilus* system secreted tube protein into extracellular space. Immunoblotting detected tube protein (Hcp), but no sheath, in the supernatant of a culture (fig. S3), indicating Hcp translocation. The system thus fulfills the functional hallmark of canonical T6SSs. Together with the structural data, this suggests that the *Amoebophilus* Afp-like gene cluster encodes a T6SS rather than an eCIS.

Next, we investigated the function of T6SS arrays. Amoebophili were internalized in the first 2 hours postinfection (hpi) and exited the amoebae ~144 hpi (fig. S4). To observe intracellular amoebophili by ECT, we used cryo-focused ion beam milling to generate lamellae that were suitable for ECT (fig. S5) (*15*, *16*). At 0.25 hpi, coccoid amoebophili were inside phagosomes (80%, n = 20; Fig. 3A and movie S7). At later stages, most amoebophili had escaped into the cytosol (94%, n = 94), differentiated into rods, and replicated (Fig. 3, B to D; fig. S6A; and movies S8 to S10). The sheath mRNA level was 230-fold higher in extracellular amoebophili compared to the replicative stage (table S2). Likewise, cryotomograms of amoebophili from different infection stages showed that T6SSs were most abundant in extracellular amoebophili (58%, n = 19) and at early infection stages (1 hpi, 96%, n = 25; 2 hpi, 69%, n = 13), whereas replicative amoebophili

[1]Institute of Molecular Biology and Biophysics, Eidgenössische Technische Hochschule Zürich, CH-8093 Zürich, Switzerland. [2]Division of Microbial Ecology, University of Vienna, A-1090 Vienna, Austria.
*These authors contributed equally to this work. †Present address: CeMM Research Center for Molecular Medicine of the Austrian Academy of Sciences, 1090 Vienna, Austria. ‡Present address: National Institute of Allergy and Infectious Diseases, Hamilton, MT 59840, USA. §Corresponding author. Email: horn@microbial-ecology.net (M.H.); pilhofer@biol.ethz.ch (M.P.)

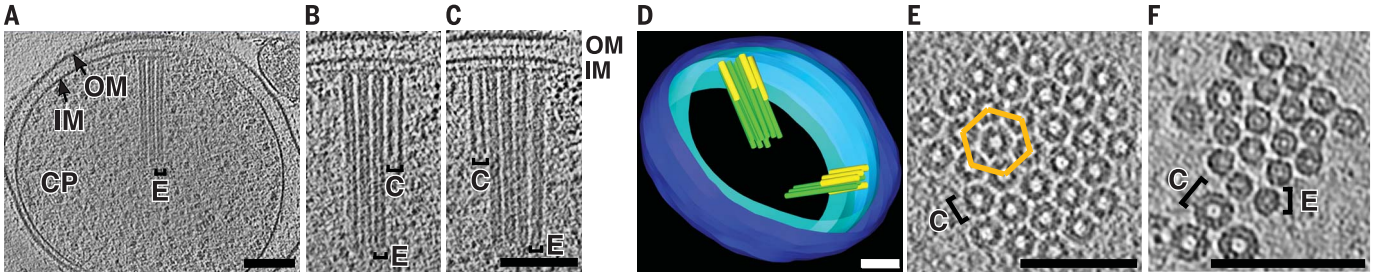

Fig. 1. The *Amoebophilus* Afp-like gene cluster encodes ordered arrays of T6S-like structures. (**A** to **C**) Cryotomograms of purified *Amoebophilus* cells revealed bundles of cytoplasmic, membrane-bound, contractile structures in extended ("E") and contracted ("C") conformations. CP, cytoplasm; IM, inner membrane; OM, outer membrane. Shown are three different 14-nm slices through the same tomogram. (**D**) Bundles comprised 2 to 34 individual machines (green, extended; yellow, contracted) and were organized in one or two bundles per cell. Shown is a model of the tomogram shown in (A) to (C). Blue, outer membrane; cyan, inner membrane. (**E** and **F**) Structures were arranged in hexagonal arrays (lattice indicated in orange). Shown are 15-nm (E) and 8-nm (F) cross-sectional slices. Bars: 100 nm.

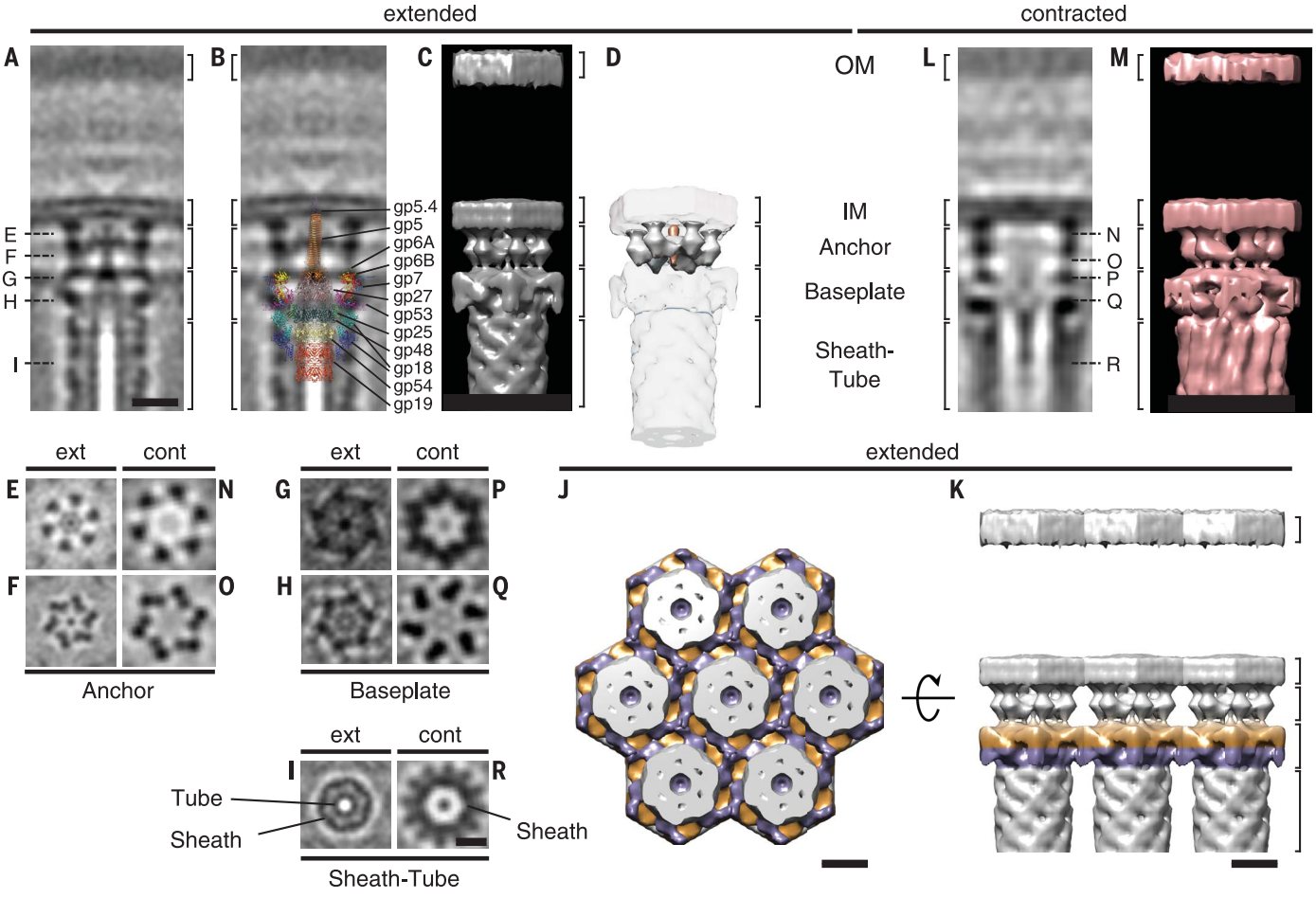

Fig. 2. The T6SS in situ architecture reveals three major modules, conformational changes upon firing, and the structural basis of array formation. Subtomogram averages of extended (**A** to **K**) and contracted (**L** to **R**) T6SSs revealed three major cytoplasmic modules: Sheath-Tube, Baseplate, and Anchor (indicated by brackets). Shown are 0.81-nm [(A) and (B), (E) to (I)] and 1.38-nm [(L), (N) to (R)] longitudinal [(A), (B), and (L)] and perpendicular [(E) to (I), (N) to (R)] slices through sixfold rotationally symmetrized averages, and their three-dimensional models [(C), (D), (J), (K), and (M)]. The positions of perpendicular sections are indicated in (A) and (L). OM, outer membrane; IM, inner membrane. Bars: 10 nm [(A) to (D), (L), and (M) to scale; (E) to (I), (N) to (R) to scale]. The segmentation in three modules was supported by the overlay (B) with the structure of the minimal composition of a contractile injection system derived from the T4 phage tail [from (*13*)]. It allowed the putative assignment of densities corresponding to tube (gp19/gp48/gp54), sheath (gp18), spike complex (gp5/gp5.4/gp27), and baseplate wedge components (gp6/gp7/gp25/gp53). Densities that were not accounted for were assigned to the anchor module [segmented in (D); white, anchor; orange, spike]. Upon firing, pronounced conformational changes were detected in all modules [movie S6 shows a morph between models shown in (C) and (M)]. The sheath increased in diameter and formed surface ridges [(A), (C), (I), (L), (M), and (R)]. Baseplate and anchor showed widening and loss of densities in the center [(A), (C), (E) to (H), (L), (M), (N) to (Q)]. Ordered arrays were established by lateral interactions of the hexagonal baseplates [(J) and (K)]. Shown are top (J) and side (K) views of a model that was assembled from masked averages. For viewing purposes, two different baseplate levels are colored in purple and orange.

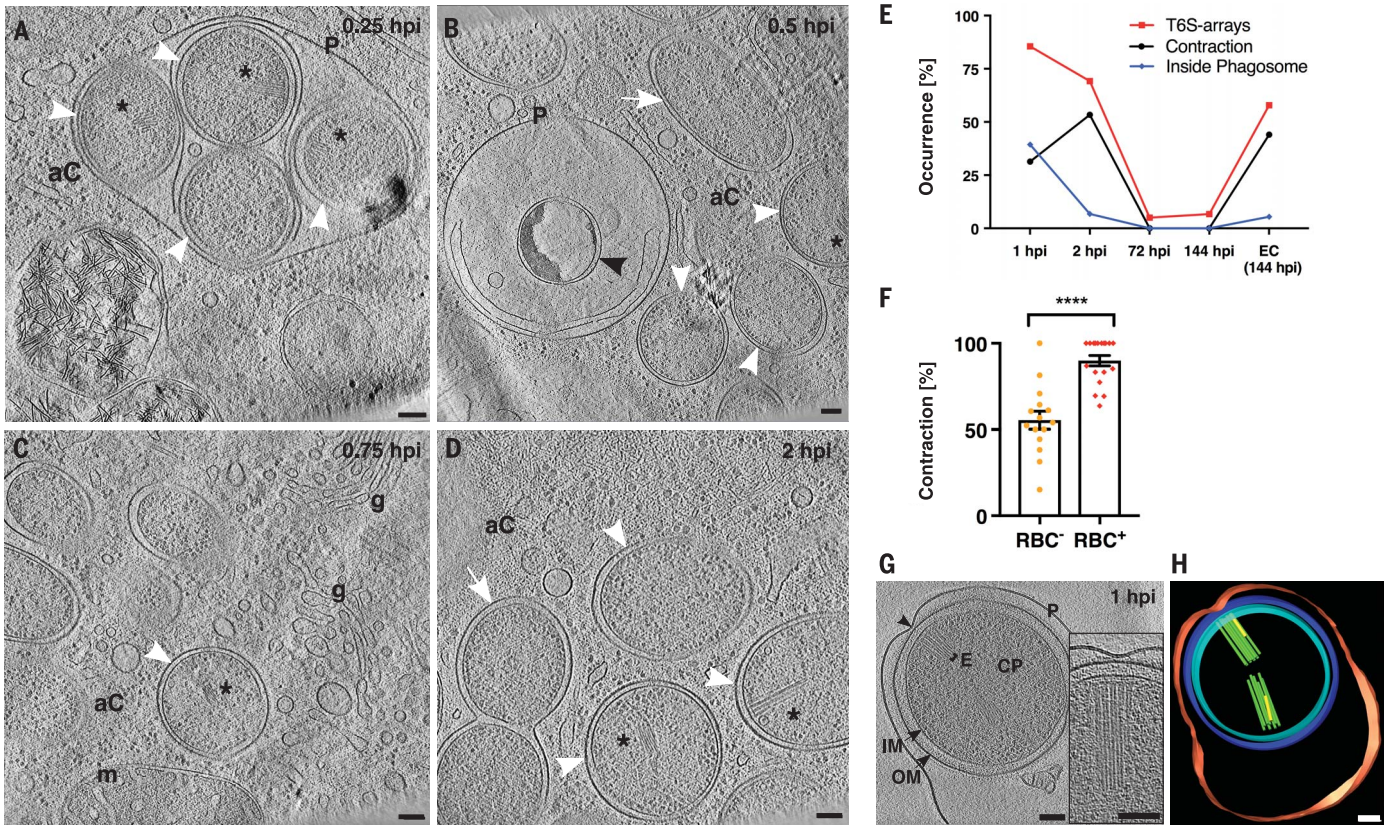

Fig. 3. T6S arrays are required during early infection stages and mediate interactions with host membranes. (**A** to **D**) Bacteria inside their host were imaged by cryo-focused ion beam milling and ECT (fig. S5). At 0.25 hpi, most coccoid amoebophili (white arrowheads) were found inside phagosomes (P). At later time points (0.5 to 2 hpi), amoebophili had escaped into the amoeba cytosol (aC). Amoebophili differentiated into rods (white arrows) and divided. A small fraction did not escape, showing signs of degradation (black arrowhead). Shown are 15-nm slices through cryotomograms. Asterisk, T6S array; g, golgi apparatus; m, mitochondrion. Bars: 100 nm. (**E**) Abundance of T6S arrays was determined by ECT of amoebophili purified from synchronized cultures, and found to be highest in extracellular "EC (144 hpi)" and early intracellular infection stages (1 hpi, 2 hpi). The increase in the contraction rate between 1 and 2 hpi correlated with the escape from the phagosome. Shown are the percentages of cells with T6S arrays (red), percentages of T6S structures that were contracted (black), and percentages of cells found inside phagosomes (blue). T6S arrays, number of quantified amoebophili: n^{1hpi} = 25, n^{2hpi} = 13, n^{72hpi} = 20, n^{144hpi} = 15, $n^{EC(144\ hpi)}$ = 19; Contraction, number of quantified T6S structures: n^{1hpi} = 168, n^{2hpi} = 88, n^{72hpi} = 4, n^{144hpi} = 4, $n^{EC(144\ hpi)}$ = 59; Inside Phagosome, number of quantified amoebophili: n^{1hpi} = 121, n^{2hpi} = 118, n^{72hpi} = 218, n^{144hpi} = 337, $n^{EC(144\ hpi)}$ = 55). (**F**) Amoebophili showed hemolytic activity (fig. S7). Extracellular amoebophili that interacted with RBCs showed an increased T6S contraction rate (****P < 0.0001; n^{RBC^-} = 506; n^{RBC^+} = 480; mean ± SEM). (**G** and **H**) Amoebophili residing in phagosomes revealed contact sites (black arrowhead) between the *Amoebophilus* outer membrane and the phagosome. Any such contact site correlated with a T6S array (n = 14). Shown are a 15-nm tomographic slice (G) and the corresponding model (H). P/red, phagosome; OM/blue, outer membrane; IM/cyan, inner membrane; CP, cytoplasm; E/green, extended T6SS; yellow, contracted T6SS; Bars: 100 nm.

did usually not harbor structures (5%, n = 20) (Fig. 3E and fig. S6, B to G). The process of exiting the phagosome during early infection (up to 2 hpi) correlated with increased fractions of contracted structures (Fig. 3E). Experiments comparing the potential of amoebophili from different infection stages to establish new infections showed that host infection rates positively correlated with T6SS expression (fig. S6H). Likewise, we tested amoebophili from different infection stages for hemolytic activity and found that red blood cell (RBC) lysis also positively correlated with T6SS expression (fig. S7). ECT imaging of amoebophili that had the possibility to interact with RBCs showed a 30% increased fraction of contracted structures, compared to a control sample (Fig. 3F; P < 0.0001). The analysis of tomograms of purified amoebophili that were found inside phagosomes (39% at 1 hpi) revealed that any contact site between the phagosome membrane and the outer membrane of the bacterium correlated with the presence of T6SSs (with at least one contracted structure) (n = 14; Fig. 3, G and H; fig. S8; and movie S11). Together, our data suggest that T6S arrays mediate interactions with host membranes and may participate in phagosome escape. It remains open whether phagosome rupturing is mediated by mechanical forces or membrane-targeting effectors.

Next, we sought to understand the evolutionary history of the *Amoebophilus* Afp-like gene cluster. We compared three key components (sheath, tail tube, baseplate component gp25) to other CISs (table S3). Similarities were highest with a gene cluster of unknown function in the related symbiont *Cardinium hertigii* (*17*). Moderate similarities were found for Afps and MACs, both mediating interactions with animal larvae (*3*, *4*). Lowest (or no similarities at all) were detected for T6SSs [subtypes *i*, *ii*, *iii* (*18*)] and contractile phages. Likewise, phylogenetic analyses revealed that *Amoebophilus* (and *Cardinium*) sequences stably clustered in a monophyletic group with Afps and MACs, rather than with $T6SS^{i\text{-}iii}$ (Fig. 4A and fig. S9). With the exception of gp7, the analysis of gene content detected *Amoebophilus* homologs of all components that are conserved across CISs and phages (*13*). These include putative sheath (gp18/TssBC), inner tube (gp19/Hcp, gp48, gp54), spike (gp5/VgrG, gp5.4/PAAR, gp27), and three baseplate wedge components (gp6/TssF, gp25/TssE, gp53) (Fig. 4B and table S4). The lack of gp7 might be explained by the presence of two gp6 homologs, and the suggestion that gp6 and gp7 diverged from a common ancestor (*13*, *19*).

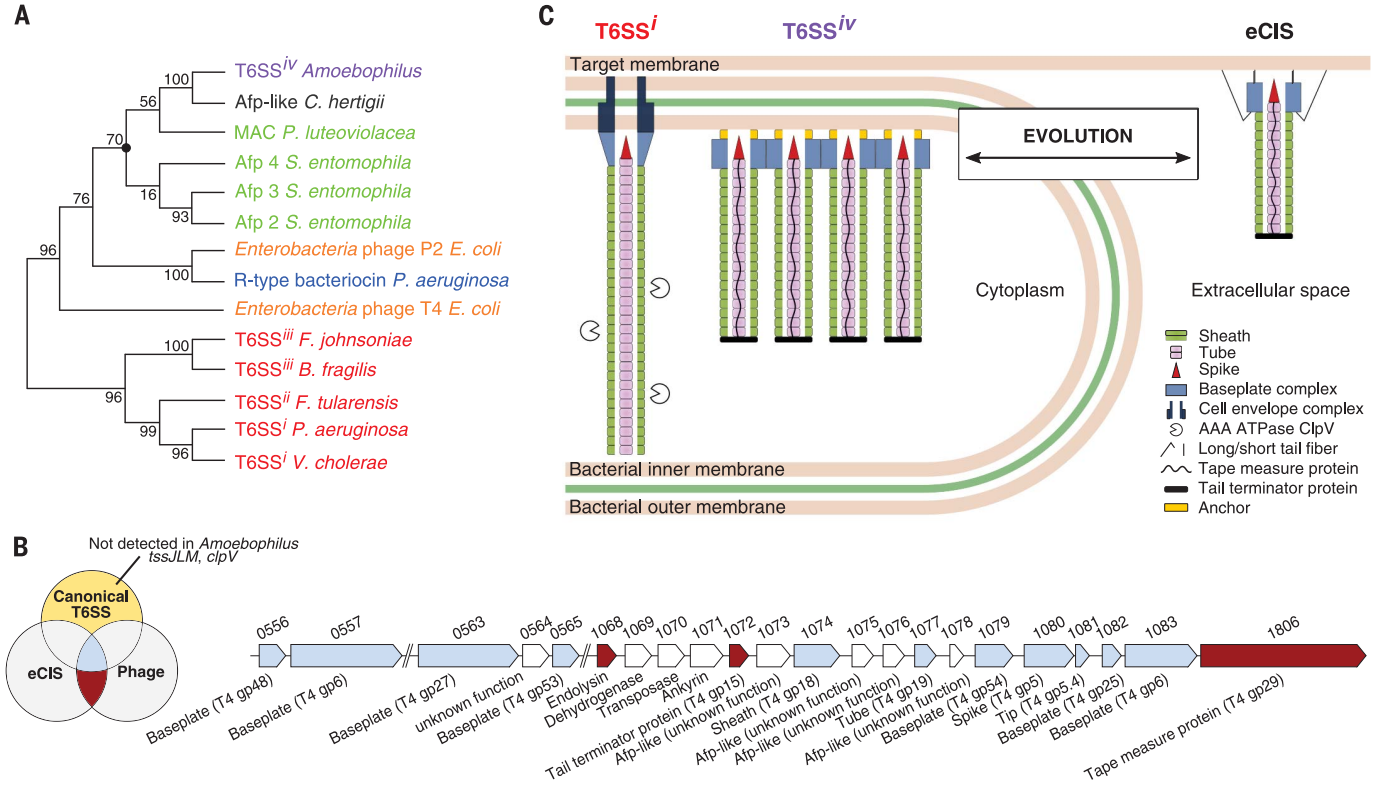

Fig. 4. *Amoebophilus* T6SS^{iv} is closely related to eCIS. (**A**) Phylogenetic analyses of sheath protein sequences showed that T6SS$^{i\text{-}iii}$ formed a monophyletic group with high support (bootstrap supports are indicated at nodes). *Amoebophilus* T6S sheath, however, stably clustered in a group with the sheath from a gene cluster in *Cardinium* (structure and function unknown), and with the eCIS sheaths of Afp and MAC. The marked node was stable in all calculated trees as determined with different treeing methods and different components (fig. S9). (**B**) The *Amoebophilus* Afp-like gene cluster encodes all components that are conserved (blue) among all contractile injection systems (canonical T6SS/eCIS/phages), although it lacks any homologs of components that are specific for canonical T6SSs (yellow). Instead, the cluster harbors genes that are typical of eCISs and phages (red). Shown are two *Amoebophilus* genomic regions, locus tags, and gene annotations. See also table S4. (**C**) Schematic showing the major components of canonical T6SS, *Amoebophilus* T6SS^{iv}, and eCIS (homologs in same colors). T6SS^{iv} evolved either from eCISs, or alternatively, T6SS^{iv} represents a primordial system that gave rise to eCISs/phages/T6SS$^{i\text{-}iii}$. Both scenarios predict that T6SSs are more abundant than previously estimated (table S5).

Components that are exclusively conserved in canonical T6SSs (and absent in eCISs/phages) were not found, including TssJLM [trans-envelope complex (*9*)] or ClpV [sheath recycling (*20*)]. By contrast, the *Amoebophilus* cluster encodes proteins that were thought to be specific for eCISs and contractile phages. The length of the *Amoebophilus* T6SSs, for instance, is likely controlled by Aasi_1072/1806, which are homologs of tail terminator and tape measure proteins in Afps and phages (*21*, *22*). Indeed, sheath length can be predicted from TmP sequence (*22*) and correlates well with the length of *Amoebophilus* sheaths (fig. S10). Another example is an Rz-like endopeptidase (Aasi_1068), which usually co-occurs with a holin to mediate the release of eCISs and phages from the bacterial cytoplasm (*3*, *23*).

In conclusion, our structural and functional data showed that the *Amoebophilus* Afp-like gene cluster encodes a T6SS, whereas sequence analyses indicated a close relationship to eCISs. We therefore introduce the term "T6SS subtype 4" (T6SS^{iv}). In contrast to the distant relationships of T6SS$^{i\text{-}iii}$ to eCISs and phages that obstruct the reconstruction of an evolutionary path (*1*, *24*), we can hypothesize that T6SS^{iv} evolved from an Afp/MAC-like eCIS (independently of T6SS$^{i\text{-}iii}$) by the loss of tail fibers, loss of holin, and the establishment of interactions with the cytoplasmic membrane. Alternatively, T6SS^{iv} represents a primordial system from which eCISs, phages, and T6SS$^{i\text{-}iii}$ have evolved (Fig. 4C). Both scenarios predict that T6SSs are more abundant than previously thought. Indeed, T6SS^{iv}-like gene clusters were detected in six diverse bacterial phyla (table S5). The finding that diverse T6SS subtypes do not share a conserved gene set that would distinguish them from eCISs or phages emphasizes the necessity of an integrative approach to discover and characterize new systems.

REFERENCES AND NOTES

1. P. G. Leiman, M. M. Shneider, *Adv. Exp. Med. Biol.* **726**, 93–114 (2012).
2. Y. Uratani, T. Hoshino, *J. Bacteriol.* **157**, 632–636 (1984).
3. M. R. H. Hurst, T. R. Glare, T. A. Jackson, *J. Bacteriol.* **186**, 5116–5128 (2004).
4. N. J. Shikuma *et al.*, *Science* **343**, 529–533 (2014).
5. M. Basler, M. Pilhofer, G. P. Henderson, G. J. Jensen, J. J. Mekalanos, *Nature* **483**, 182–186 (2012).
6. A. Hachani, T. E. Wood, A. Filloux, *Curr. Opin. Microbiol.* **29**, 81–93 (2016).
7. Y.-W. Chang, L. A. Rettberg, D. R. Ortega, G. J. Jensen, *EMBO Rep.* **18**, 1090–1099 (2017).
8. M. Basler, *Philos. Trans. R. Soc. London B Biol. Sci.* **370**, 20150021 (2015).
9. E. Durand *et al.*, *Nature* **523**, 555–560 (2015).
10. M. Horn *et al.*, *Environ. Microbiol.* **3**, 440–449 (2001).
11. S. Schmitz-Esser *et al.*, *J. Bacteriol.* **192**, 1045–1057 (2010).
12. T. Penz, M. Horn, S. Schmitz-Esser, *Virulence* **1**, 541–545 (2010).
13. N. M. I. Taylor *et al.*, *Nature* **533**, 346–352 (2016).
14. M. M. Shneider *et al.*, *Nature* **500**, 350–353 (2013).
15. M. Marko, C. Hsieh, R. Schalek, J. Frank, C. Mannella, *Nat. Methods* **4**, 215–217 (2007).
16. A. Rigort *et al.*, *J. Struct. Biol.* **172**, 169–179 (2010).
17. T. Penz *et al.*, *PLOS Genet.* **8**, e1003012 (2012).
18. A. B. Russell *et al.*, *Cell Host Microbe* **16**, 227–236 (2014).
19. C. R. Büttner, Y. Wu, K. L. Maxwell, A. R. Davidson, *Proc. Natl. Acad. Sci. U.S.A.* **113**, 10174–10179 (2016).
20. G. Bönemann, A. Pietrosiuk, A. Diemand, H. Zentgraf, A. Mogk, *EMBO J.* **28**, 315–325 (2009).
21. D. Rybakova *et al.*, *Mol. Microbiol.* **89**, 702–714 (2013).
22. D. Rybakova, P. Schramm, A. K. Mitra, M. R. H. Hurst, *Mol. Microbiol.* **96**, 815–826 (2015).
23. I. N. Wang, D. L. Smith, R. Young, *Annu. Rev. Microbiol.* **54**, 799–825 (2000).
24. P. G. Leiman *et al.*, *Proc. Natl. Acad. Sci. U.S.A.* **106**, 4154–4159 (2009).

ACKNOWLEDGMENTS

We thank F. Bosia, A. Harreither, P. Gasser, S. Rutz, P. Szwedziak, P. Tittmann, R. Wepf, and C. Zaubitzer for technical support. ScopeM is acknowledged for instrument access at ETH Zürich. We thank O. Medalia for microscope access at the University of Zürich. T. Ishikawa, R. Wepf,

and Pilhofer Lab members are acknowledged for discussions. R. Kostanjsek is acknowledged for generating preliminary data. W.-D. Hardt, H. Hilbi, R. Kooger, V. Panse, N. Shikuma, M. Swulius, and E. Tocheva are acknowledged for comments on the manuscript. We thank N. Taylor for providing us with the T4 model shown in Fig. 2B. Preliminary observations were made in the lab of G. J. Jensen. M.P. is supported by the European Research Council, the Swiss National Science Foundation, and the Helmut Horten Foundation. M.H. is supported by the European Research Council (ERC StG, no. 281633) and Austrian Science Fund (I 1628-B22). Subtomogram averages and tomograms were deposited in the Electron Microscopy Data Bank (accession numbers EMD-3791 and EMD-3793 to EMD-3801).

SUPPLEMENTARY MATERIALS

www.sciencemag.org/content/357/6352/713/suppl/DC1

19 May 2017; accepted 17 July 2017
10.1126/science.aan7904

Science

In situ architecture, function, and evolution of a contractile injection system

Désirée Böck, João M. Medeiros, Han-Fei Tsao, Thomas Penz, Gregor L. Weiss, Karin Aistleitner, Matthias Horn and Martin Pilhofer

Science **357** (6352), 713-717.
DOI: 10.1126/science.aan7904

Identification of a new injection system

To interact with other cells, bacteria use contractile machines that function similarly to membrane-puncturing bacteriophages. The so-called type 6 secretion system (T6SS) functions from inside a bacterial cell. Böck *et al.* used modern electron microscopy methods and functional assays to resolve the structure and function of a T6SS in the cellular context. They identified three modules and showed large-scale structural changes upon firing. T6SSs are organized in multibarrel gun-like arrays and may contribute to the survival of bacteria inside their host.

Science, this issue p. 713